Slow Magnetic Relaxation in a Heteroleptic Anilate-based Dy^{III} Metal-Organic Framework

Mariangela Oggianu,[a] Federica Bertolotti,[b] Fabio Manna,[a,d] Francesco Congiu,[c] Antonio Cappai,[c] Claudio Melis,[c] Giorgio Concas,[c] Narcis Avarvari,[d] Norberto Masciocchi[b] and Maria Laura Mercuri*[a]

[a]Dipartimento di Scienze Chimiche e Geologiche, Università degli Studi di Cagliari, I-09042 Monserrato, Italy.

[b]Dipartimento di Scienza e Alta Tecnologia & To.Sca.Lab., Università dell'Insubria, via Valleggio 11, 22100 Como, Italy.

[c]Dipartimento di Fisica, Università degli Studi di Cagliari, S. P. Monserrato-Sestu km 0,700, I-09042 Monserrato (CA), Italy.

[d]Laboratoire MOLTECH-Anjou UMR 6200, UFR Sciences, CNRS, Université d'Angers, Bât. K, 2 Bd. Lavoisier, 49045 Angers, France.

Summary

1. Results and Discussion
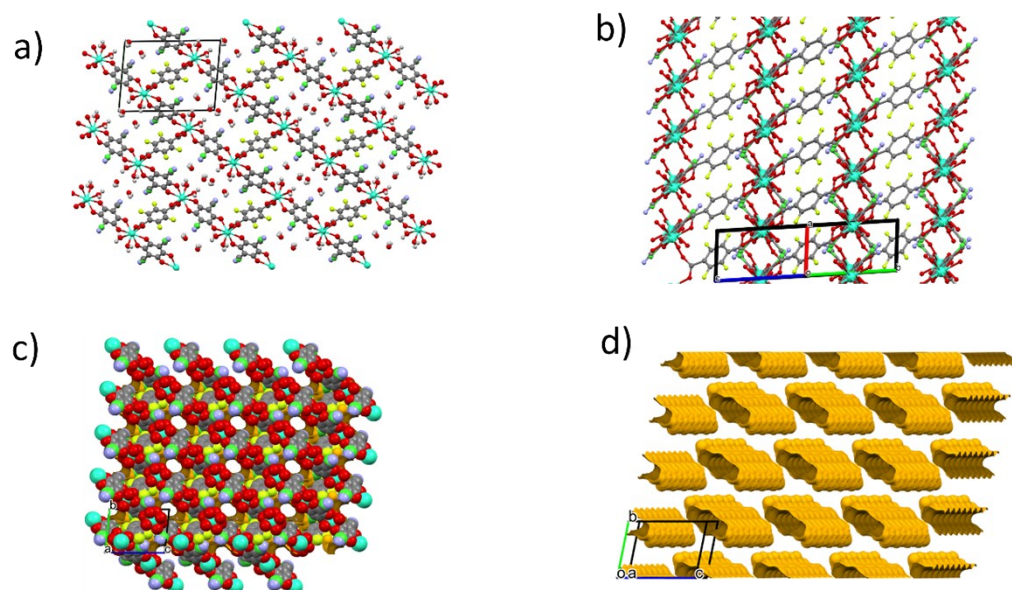
1.1 Structural Characterization

Figure S1. a) The crystal structure of **1** viewed down the **a** axis, in which the arrangement of water molecules in the channels can be seen; b) representation of the 1D chains of Tb^{III} ions bridged by the F_4BDC^{2-} moieties; c) space-filling model of **1**, highlighting the voids generated by removal of non-coordinated water molecules; d) Mercury representation of the size/shape of the voids. Colour codes: C, grey; N, blue; O, red; F, yellow; Cl, green; Tb, cyan.
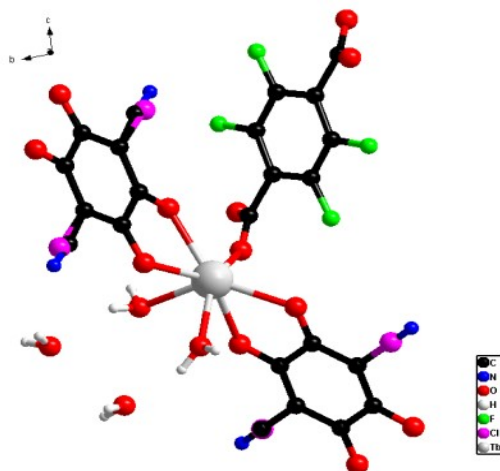

Figure S2. The coordination sphere around the Ln^{III} ions (coordinates taken from the single-crystal structure model of **1**). Site occupancy factors for Cl1, Cl2, N1, N2, C4, C12 atoms = 0.5.

Table S1. Crystal data and structure refinement parameters for **1.**

Empirical formula	$C_{11}H_8ClF_2NO_{10}Tb$
Formula weight, amu	546.55
Temperature	200.0(1) K
Wavelength	1.54184 Å
Crystal system, space group	Triclinic, $P\bar{1}$
Unit cell dimensions	a = 5.1017(3) Å α = 95.724(4) °
	b = 10.7630(6) Å β = 99.786(5) °
	c = 14.8712(8) Å γ = 90.157(5) °
Cell volume	800.52(8) Å^3
Z, Calculated density	2, 2.267 Mgm^{-3}
Absorption coefficient	24.020 mm^{-1}
F(000)	522
Crystal size	0.13 x 0.03 x 0.03 mm – red needle
θ range for data collection	3.031 - 71.888 °
Limiting indices	6≤h≤6, -10≤k≤13, -18≤l≤18
Reflections collected / unique	6434 / 3081 [R(int) = 0.0566]
Completeness to θ = 71.00°	98.5 %
Absorption correction	Semi-empirical from equivalents
Max. and min. transmission	1.000 and 0.427
Refinement method	Full-matrix least-squares on F^2
Goodness-of-fit on F^2	1.072
Final R indices [I>2σ(I)]	R1 = 0.0489, wR2 = 0.1234 [2858 Fo]
R indices (alldata)	R1 = 0.0527, wR2 = 0.1276
Largest diff. peak and hole	1.952 and -1.323 e Å^3

Table S2. Selected bond distances for **1** (Å). Esd's in parentheses.

Tb1-O1 2.463(5)	Tb1-O5 2.437(4)	Tb1···Tb1 5.1017(5) (carboxylate-bridged)
Tb1-O2 2.389(4)	Tb1-O6 2.443(4)	Tb1···Tb1 8.7448(6) (anilate-bridged)
Tb1-O3 2.280(4)	Tb1-O7 2.365(4)	C1-O1 1.264(8) C9-O5 1.249(9)
Tb1-O4 2.310(5)	Tb1-O8 2.383(5)	C2-O2 1.247(8) C11-O6 1.265(7)

Table S3. Synoptic collection of lattice metrics for compounds **1**-**3** and their known Yb and Er analogues.

Compound	CR[a], Å	a, Å	b, Å	c, Å	α, °	β, °	γ, °	V, Å^3
(Yb)[1]	1.125	5.07	10.77	14.65	95.9	99.7	90.5	784
(Er)[1]	1.144	5.11	10.78	14.73	95.8	99.7	90.5	795
3 (Ho)	1.155	5.13	10.83	14.74	95.7	99.7	90.5	804
2 (Dy)	1.167	5.15	10.82	14.80	95.7	99.7	90.3	808
1 (Tb)	1.180	5.16	10.80	14.91	95.8	99.8	90.2	814

[a] Shannon's crystal radii.[2]

1.2 Thermo-Gravimetric Analysis (TGA)

TGA was performed on polycrystalline samples of **1**, **2** and **3** (Figure S3). The first weight loss occurring at 70 °C (about 3-4%) is due to the elimination of surface *physisorbed* moisture, while the loss at 80-100°C (about 6%) corresponds to the removal of *clathrated* water molecules from the cavities of the MOF structures discussed in the main text. Above100 °C, **1**, **2**and**3** show an additional weight loss (of about 6–7%), attributed to the complete removal of the *coordinated* water molecules. Above 375 °C, all three compounds present a further and remarkable weight loss, due to material decomposition. Altogether, these results confirm the stoichiometry of the polycrystalline materials, which are in agreement with the water-content formulations presented in the main text from the single crystal analysis of compound **1**.
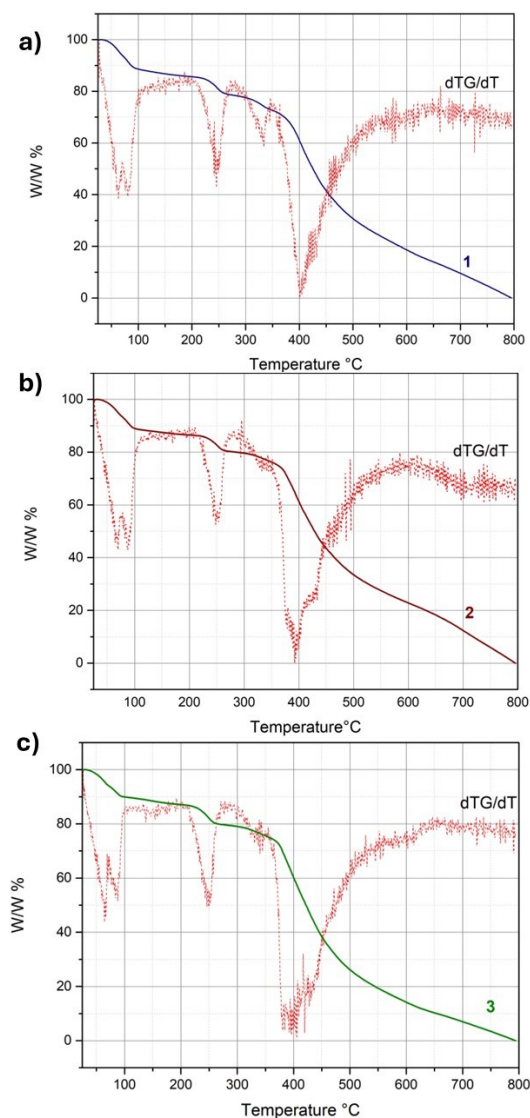

Figure S3. Thermograms of **1**, **2** and **3** in the 25−800°C range.

1.3 Fourier Transform Infrared Spectroscopy (FT-IR)

The FT-IR spectra of **1**, **2** and **3** were collected and compared with those of both **KHClCNAn** and **H₂F₄BDC** linkers. As shown in **Figure S4**, the two bands at 1780 cm⁻¹ and 1650 cm⁻¹ are assigned to the ν(CO) stretching vibration mode for the uncoordinated C=O groups of **H$_2$F$_4$BDC** and **KHClCNAn**, respectively. As shown in **Figure S9b**, in **1**, **2** and **3** this band is downshifted to 1540-1520 cm⁻¹, due to the C=O coordination to the metal ions. In the fingerprint region, the sharp band observed at 1030 cm⁻¹ in the FT-IR spectra of **1-3** can be assigned to the C-F stretching vibration which is red-shifted if compared to that of the pristine **H$_2$F$_4$BDC** linker.
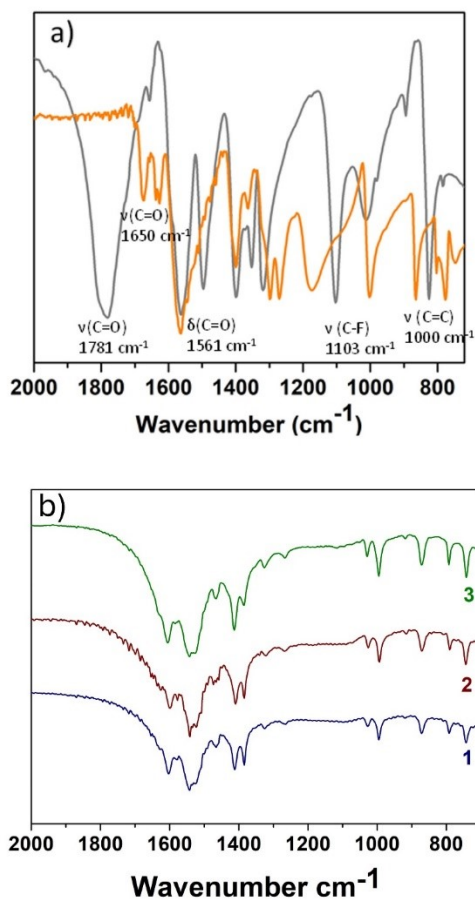

Figure S4. FT-IR spectra of: a) KHClCNAn (orange line), H₂F₄BDC (grey line) and b) **1** (red line), **2** (blue line) **3** (green line), in the 2000-700 cm⁻¹ region.

1.4 Computational Characterization

Table S4. Löwdin[3,4] charges of the oxygen atoms for the compound **2** (Dy), computed by DFT

Atom	q, electron charge units
O1	-0.363
O2	-0.313
O3	-0.333
O4	-0.322
O5	-0.310
O6	-0.326
O7	-0.561
O8	-0.575

1.5 Magnetic Characterization

Equation S1. Dy^{III} susceptibility[5]

$$\chi_{Dy} = \frac{Ng^2\beta}{kT}\left(\frac{0.5e^{-\frac{0.25\Delta}{kT}} + 4.5e^{-\frac{2.25\Delta}{kT}} + 12.5e^{-\frac{6.25\Delta}{kT}} + 24.5e^{-\frac{12.25\Delta}{kT}} +}{1 + 2e^{-\frac{\Delta}{kT}} + 2e^{-\frac{2\Delta}{kT}} + 2e^{-\frac{9\Delta}{kT}} + 2e^{-\frac{16\Delta}{kT}} + 2e^{-\frac{25\Delta}{kT}} + 2e^{-\frac{36\Delta}{kT}}}\right. + \frac{40.5e^{-\frac{20.25\Delta}{kT}} +}{1 + 2e^{-\frac{\Delta}{kT}} + 2}$$

Equation S2.Tb^{III} susceptibility[5]

$$\chi_{Tb} = \frac{Ng^2\beta}{kT}\left(\frac{2e^{-\frac{\Delta}{kT}} + 4e^{-\frac{2\Delta}{kT}} + 18e^{-\frac{9\Delta}{kT}} + 32e^{-\frac{16\Delta}{kT}} + 50e^{-\frac{25\Delta}{kT}} + 72e^{-\frac{36\Delta}{kT}}}{1 + 2e^{-\frac{\Delta}{kT}} + 2e^{-\frac{2\Delta}{kT}} + 2e^{-\frac{9\Delta}{kT}} + 2e^{-\frac{16\Delta}{kT}} + 2e^{-\frac{25\Delta}{kT}} + 2e^{-\frac{36\Delta}{kT}}}\right)$$

Equation S3.Ho^{III} susceptibility[5]

$$\chi_{Ho} = \frac{Ng^2\beta}{kT}\left(\frac{2e^{-\frac{\Delta}{kT}} + 8e^{-\frac{2\Delta}{kT}} + 18e^{-\frac{9\Delta}{kT}} + 32e^{-\frac{16\Delta}{kT}} + 50e^{-\frac{25\Delta}{kT}} + 72e^{-\frac{36\Delta}{kT}} + 98e^{-\frac{49\Delta}{kT}} + 128e^{-\frac{64\Delta}{kT}}}{1 + 2e^{-\frac{\Delta}{kT}} + 2e^{-\frac{4\Delta}{kT}} + 2e^{-\frac{9\Delta}{kT}} + 2e^{-\frac{16\Delta}{kT}} + 2e^{-\frac{25\Delta}{kT}} + 2e^{-\frac{36\Delta}{kT}} + 2e^{-\frac{49\Delta}{kT}} + 2e^{-\frac{64\Delta}{kT}}}\right)$$
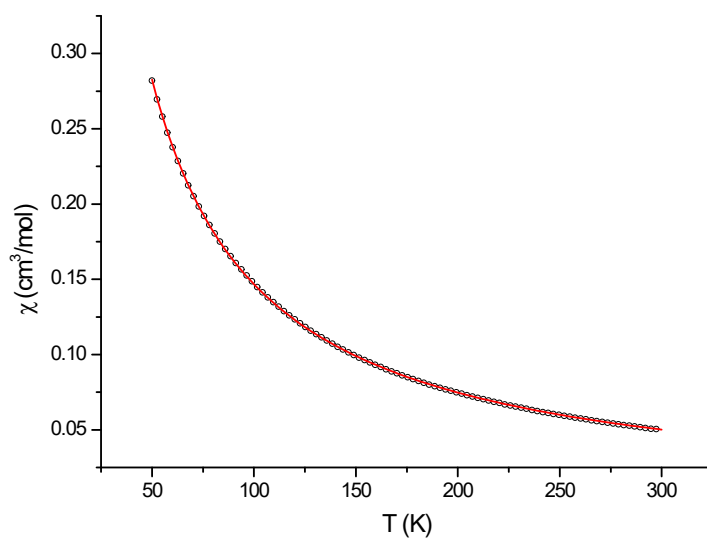
Figure S5. Molar susceptibility *vs.* temperature, with applied field of 1000 Oe, of compound **2** (Dy): experimental data (black circles) and fitting curve (red line).
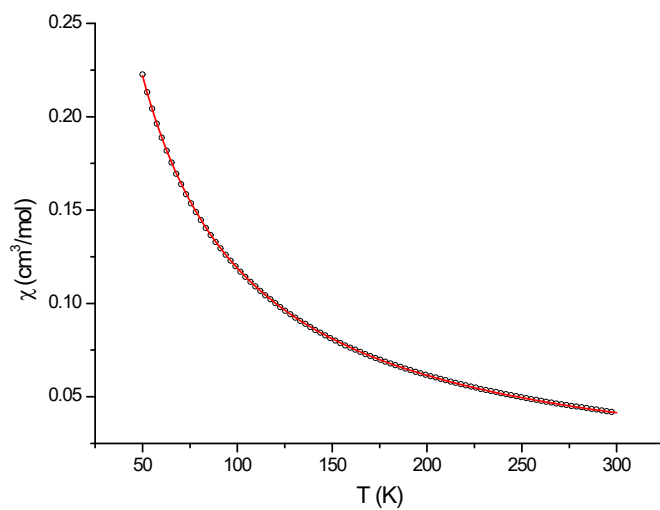

Figure S6. Molar susceptibility vs. temperature, with applied field of 1000 Oe, of compound **1** (Tb): experimental data (black circles) and fitting curve (red line).
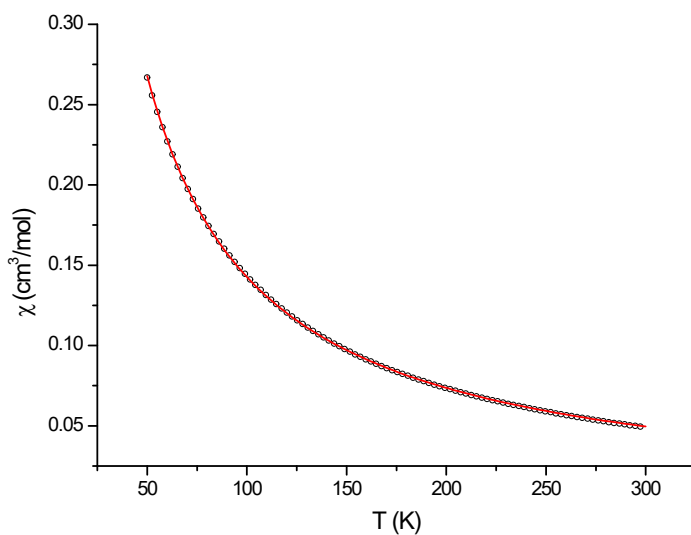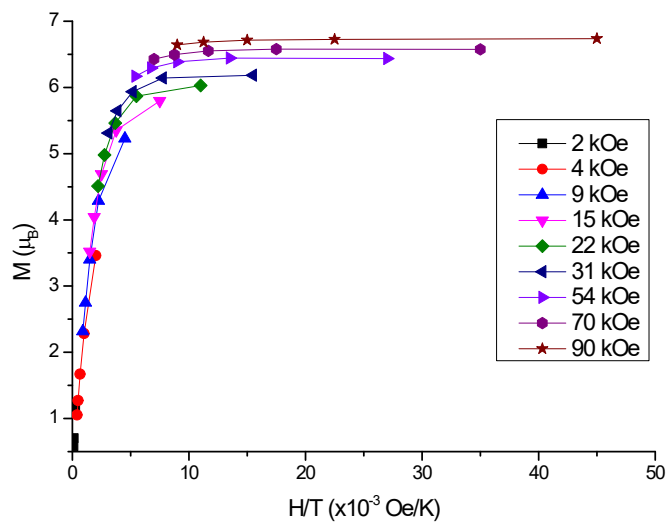
Figure S7. Molar susceptibility vs. temperature, with applied field of 1000 Oe, of compound **3** (Ho): experimental data (black circles) and fitting curve (red line).

Figure S8. Magnetization (in Bohr magnetons) vs. the field/temperature ratio of compound **2** (Dy); each curve represents the susceptibility for a given field at temperatures of 2 K, 4 K, 6 K, 8 K and 10 K.
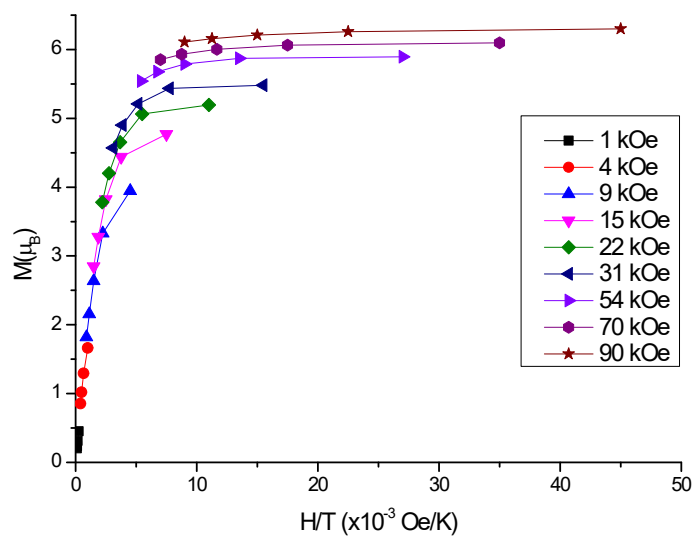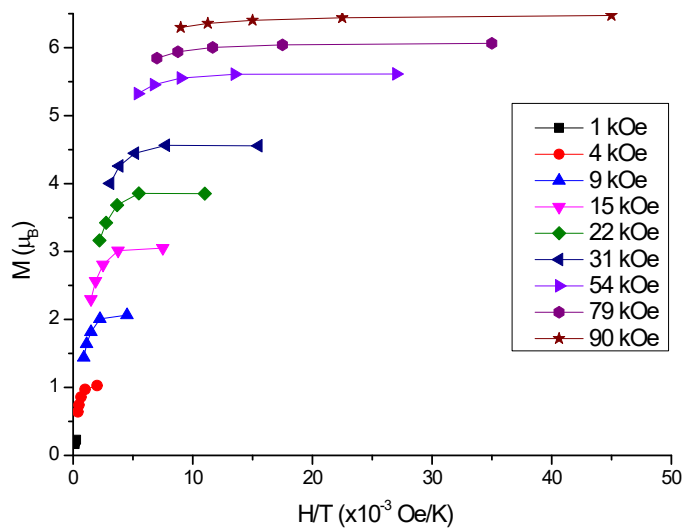
Figure S9. Magnetization (in Bohr's magnetons) vs. the field/temperature ratio of compound **1** (Tb); each curve represents the susceptibility for a given field at temperatures of 2 K, 4 K, 6 K, 8 K and 10 K.

Figure S10. Magnetization (in Bohr's magnetons) vs. the field/temperature ratio of compound **3** (Ho); each curve represents the susceptibility for a given field at temperatures of 2 K, 4 K, 6 K, 8 K and 10 K.
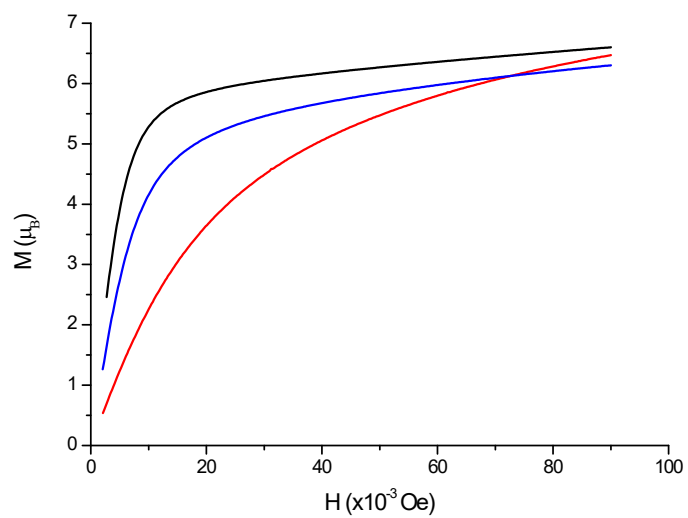
Figure S11. Magnetization at 2 K (in Bohr's magnetons) vs. applied field of compounds **1** (Tb, blue line), **2** (Dy, black) and **3** (Ho, red).
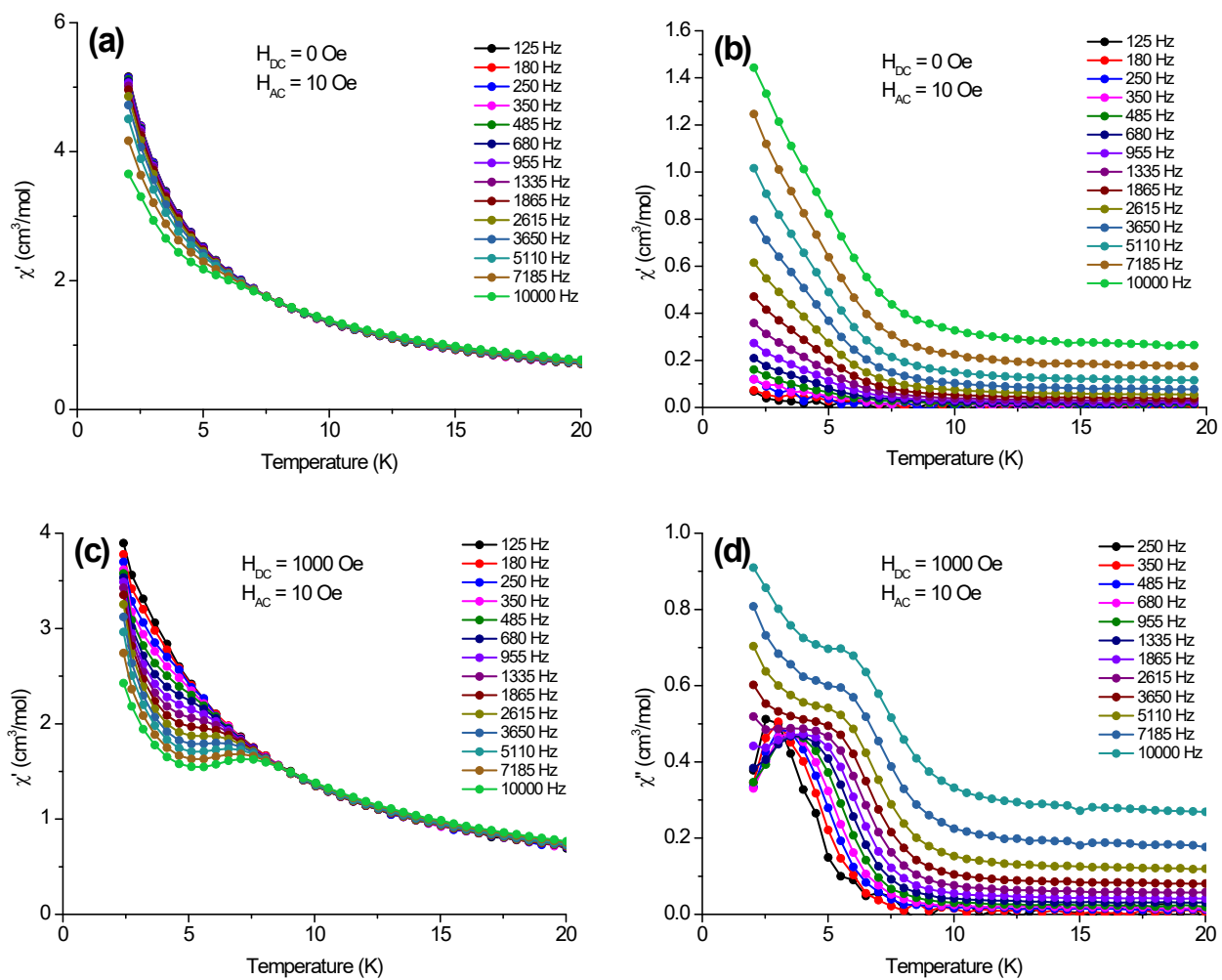
Figure S12. Temperature dependence of the in phase χ' (left) and out of phase χ'' (right) components for compound **2** (Dy) measured under H_{DC} = 0 Oe (a,b) and 1000 Oe (c,d).
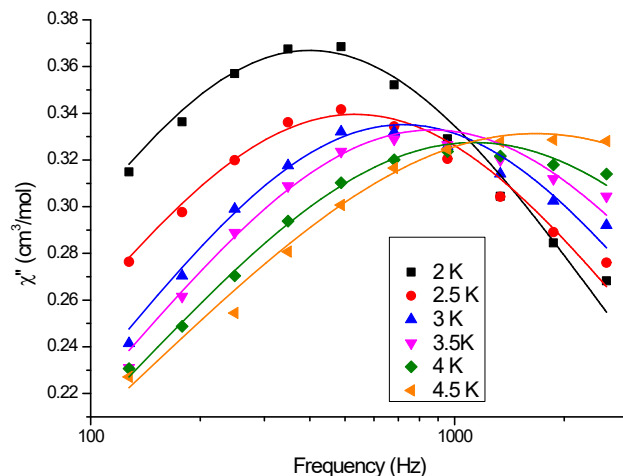
Figure S13. Frequency dependence of the out of phase component of the susceptibility for compound **2** (Dy) measured under H_{DC} = 5000 Oe. Experimental data (symbols) and best fitting curves to the generalized Debye model are shown (imaginary part of Eq. S5 below).
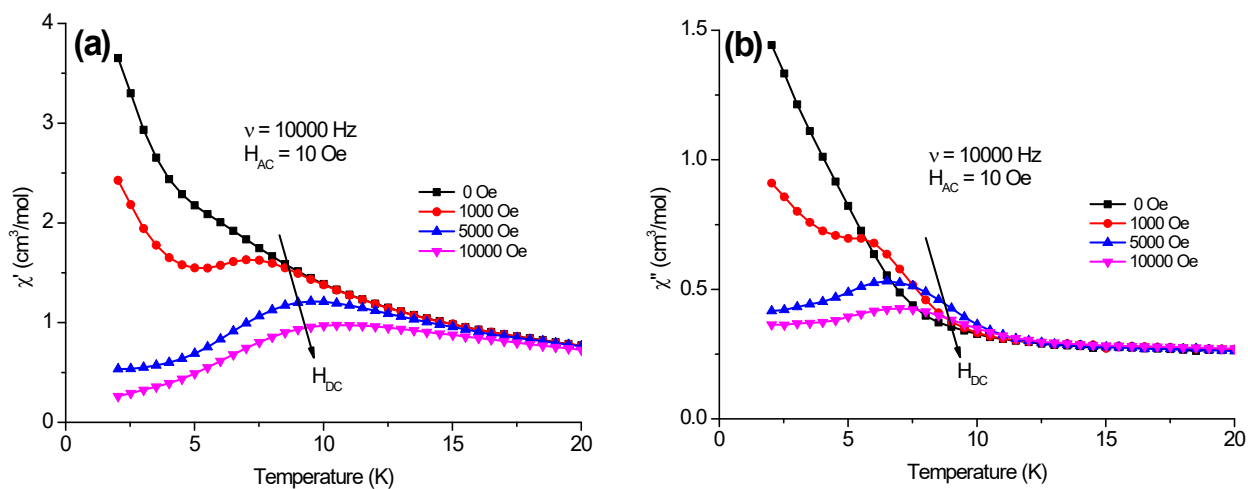

Figure S14. Temperature dependence of the in phase χ' (a) and out of phase χ'' (b) components for compound **2** (Dy) measured at ν= 10000 Hz with H_{AC} = 10 Oe and different values of H_{DC}.
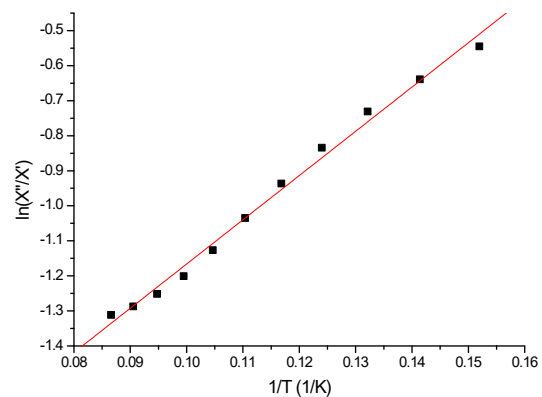
Figure S15. Linear fit for the magnetic relaxation process according to equationS4 for compound **2** (Dy). Black squares represent experimental values, the red line is the fitting curve.
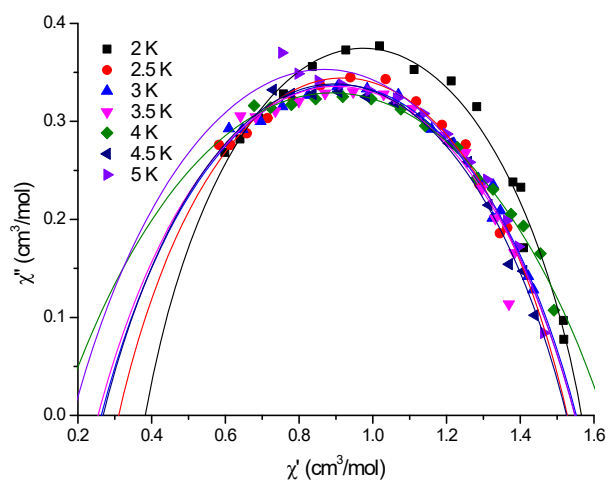

Figure S16. The Cole−Cole plot for compound **2** (Dy). The solid lines represent the best fit with equation S6.

Equation S4. χ''/χ' according to the Debye model[6]

$$\ln\frac{\chi''}{\chi'} = \ln\left(2\pi\nu\tau_0\right) + \frac{U_{eff}}{k_B T}$$

Equation S5. $\chi(\omega)$ according to the generalized Debye model[7]

$$\chi(\omega) = \chi_S + \frac{\chi_T - \chi_S}{1 - (i\omega\tau)^{(1-\alpha)}}$$

Equation S6. Fit of the Cole-Cole plots according to the generalized Debye model[7]

$$\chi'' = -\left(\frac{\chi_T - \chi_S}{2}\tan\frac{\pi\alpha}{2}\right) + \sqrt{\left(\frac{\chi_T - \chi_S}{2}\tan\frac{\pi\alpha}{2}\right)^2 + (\chi' - \chi_S)(\chi_T - \chi')}$$

Table S5. Parameters obtained by fitting the Cole-Cole plots of AC susceptibility of compound **2** measured with H_{DC} = 5000 Oe.

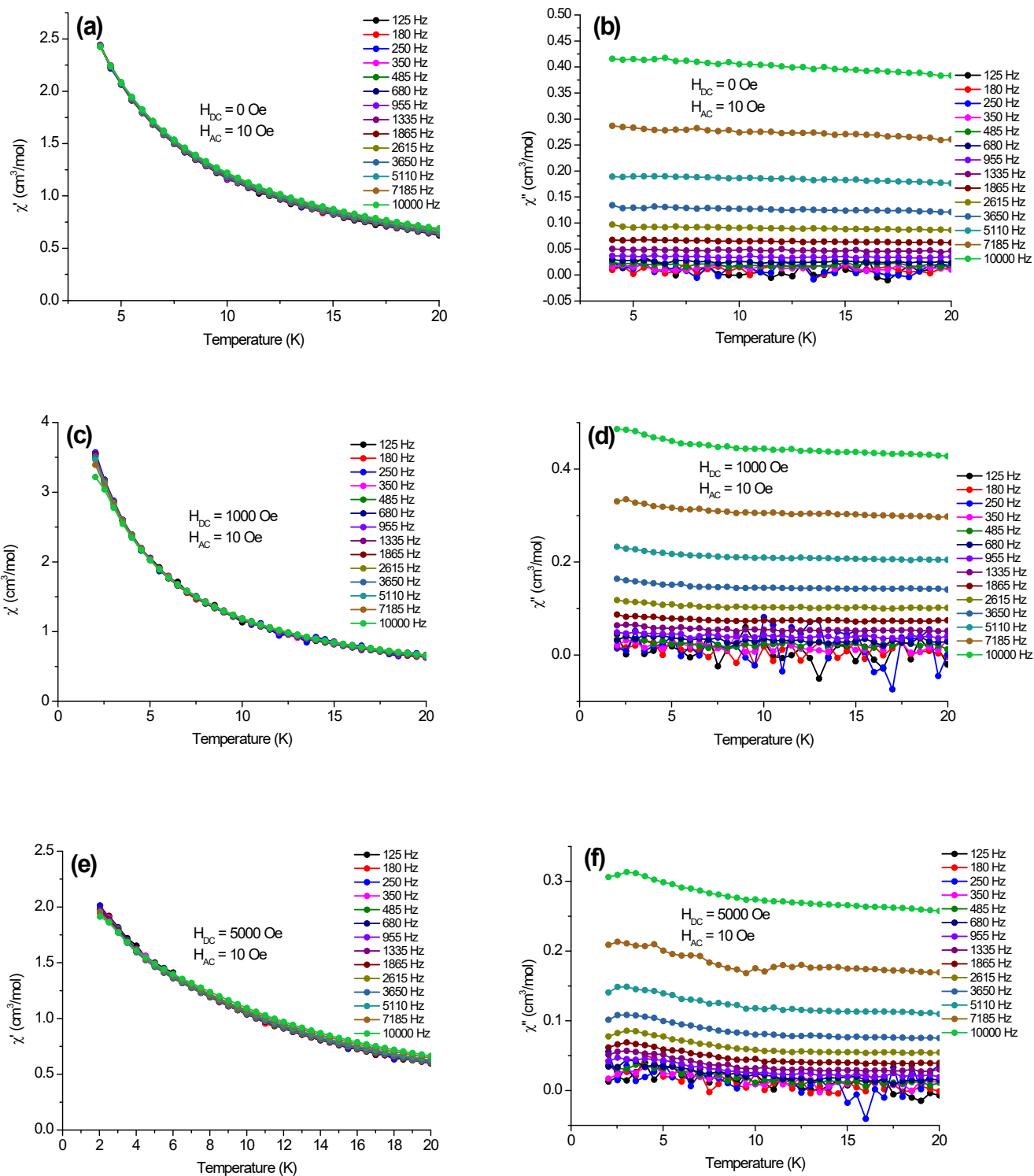| T (K)	χ_S (cm³/mol)	χ_T (cm³/mol)	α
2.0	0.38(2)	1.57(1)	0.28(2)
2.5	0.31(2)	1.53(2)	0.34(2)
3.0	0.26(3)	1.55(1)	0.39(2)
3.5	0.25(3)	1.55(2)	0.39(2)
4.0	0.15(4)	1.63(1)	0.47(2)
4.5	0.27(4)	1.53(1)	0.37(2)
5.0	0.19(8)	1.55(2)	0.39(3)

Figure S17. Temperature dependence of the in phase χ' (left) and out of phase χ'' (right) components for compound **1** (Tb) measured under H_{DC} = 0 Oe (a, b), 1000 Oe (c, d) and 5000 Oe (e, f).

Figure S18. Temperature dependence of the in phase χ' (left) and out of phase χ'' (right) components for compound **3** (Ho) measured under H_{DC} = 0 Oe (a, b), 1000 Oe (c, d) and 5000 Oe (e, f).
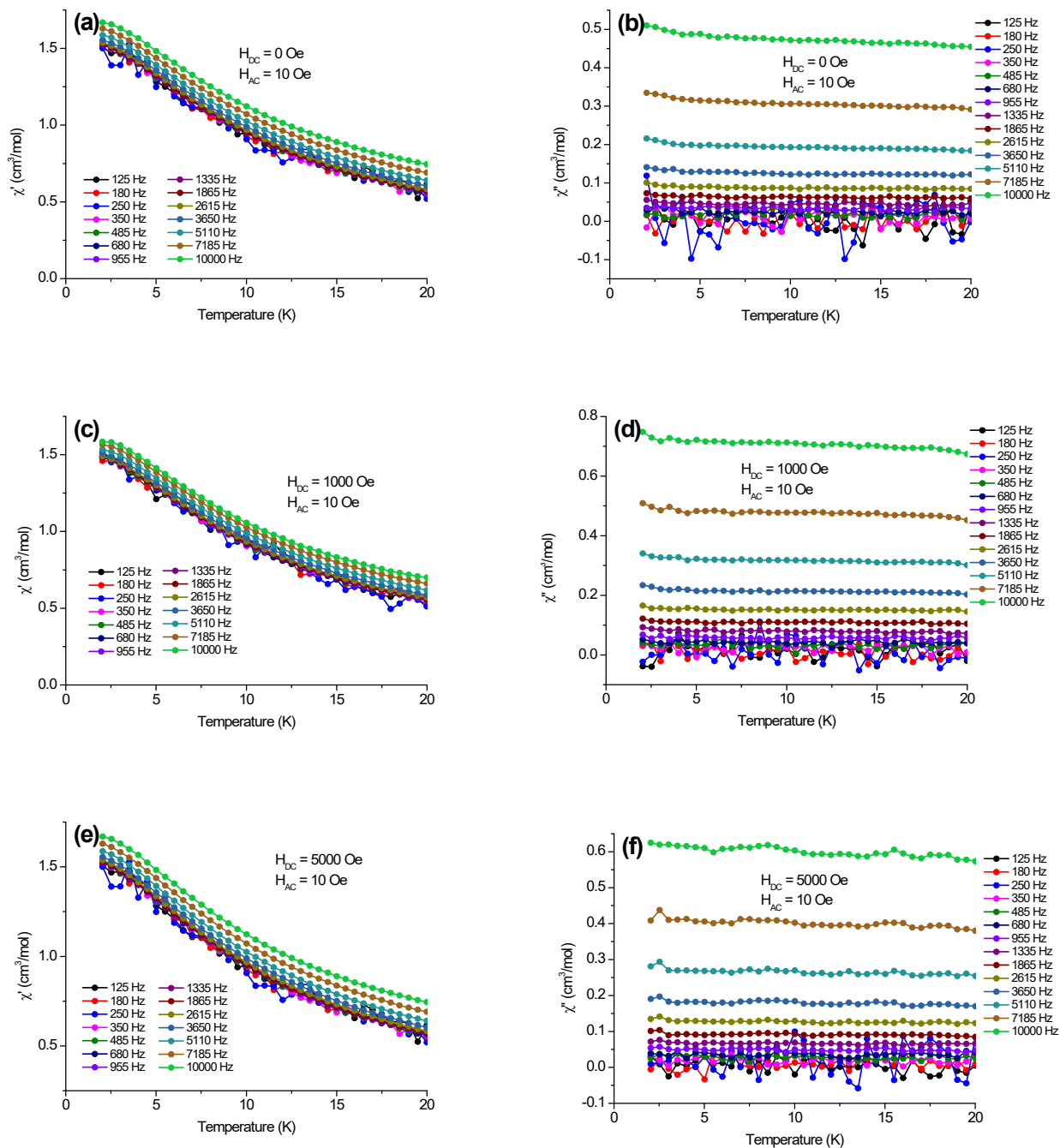
2.0 References

1   M. Oggianu, F. Manna, S. Ashoka Sahadevan, N. Avarvari, A. Abhervé and M. L. Mercuri, *Crystals*, 2022, **12**, 763.

2   R. D. Shannon, *Acta Crystallogr. Sect. A*, 1976, **32**, 751–767.

3   N. S. O. A. Szabo, *Modern Quantum Chemistry*, 1996.

4   P.-O. Löwdin, *J. Chem. Phys.*, 1950, **18**, 365–375.

5   C.-H. Zhan, F. Wang, Y. Kang and J. Zhang, *Inorg. Chem.*, 2012, **51**, 523–530.

6   E. Echenique-Errandonea, R. F. Mendes, F. Figueira, D. Choquesillo-Lazarte, G. Beobide, J. Cepeda, D. Ananias, A. Rodríguez-Diéguez, F. A. Almeida Paz and J. M. Seco, *Inorg. Chem.*, 2022, **61**, 12977–12990.

7   C. V Topping and S. J. Blundell, *J. Phys. Condens. Matter*, 2019, **31**, 013001.